SIAM J. APPL. MATH.
Vol. 73, No. 4, pp. 1703–1720




# CRIME MODELING WITH LÉVY FLIGHTS*

SORATHAN CHATURAPRUEK†, JONAH BRESLAU‡, DANIEL YAZDI§, THEODORE KOLOKOLNIKOV¶, AND SCOTT G. MCCALLA§

**Abstract.** The UCLA burglary hotspot model, introduced in [M. B. Short, M. R. D'Orsogna, V. B. Pasour, G. E. Tita, P. J. Brantingham, A. L. Bertozzi, and L. B. Chayes, *Math. Models Methods Appl. Sci.*, 18 (2008), pp. 1249–1267], models the formation of hotspots of criminal activity. In this paper, we extend the UCLA model to incorporate a more realistic model of human locomotion. The movement of the criminal agents follows a biased Lévy flight with step sizes distributed according to a power-law distribution. The biased Brownian motion of the original model is then derived as a special case. Starting with an agent-based model, we derive its continuum limit. This consists of two equations and involves the fractional Laplacian operator. A numerical method based on the fast Fourier transform is used to simulate the continuum model; these simulations compare favorably with the direct numerical simulations of the agent-based model. A Turing-type analysis is performed to estimate how the instability of the homogeneous steady state, as well as the expected number of hotspots, depends on the system parameters and especially the exponent of the underlying power law. The assumptions of the underlying agent-based model naturally lead to a separation of scales of the diffusion coefficients in the continuum limit. Using these assumptions, we asymptotically construct the leading-order profile of the localized hotspot of criminal activity.

**Key words.** fractional Laplacian, superdiffusion, hotspots, Lévy flights, crime modeling, Turing analysis

**AMS subject classifications.** 35Q91, 35Q92, 60G22

**DOI.** 10.1137/120895408

## 1. Introduction.

Crime is an unfortunate but persistent part of life in all parts of the world. Furthermore, it is not uniformly distributed; certain neighborhoods contain high levels of criminal activity in comparison to others. This can be due to socioeconomic forces, geographical structure, or even the composition of the local businesses [3, 5, 10, 25, 1, 4, 27, 36, 37, 16, 23]. Surprisingly, localized regions of unusually high crime can also occur as a result of previous crimes in the area [8, 17, 32, 24]. These regions containing elevated criminal activity are known as hotspots. In a series of pioneering works [33, 31, 30, 32], the UCLA group has proposed a mathematical model (henceforth referred to as the *UCLA model*) for understanding the dynamics of criminal activity. For simplicity, they focused on residential burglaries wherein the targets are stationary. Only the offender's movements need to be understood.

*Received by the editors October 16, 2012; accepted for publication (in revised form) June 18, 2013; published electronically August 15, 2013. This work was supported by the California Research Training Program in Computational and Applied Mathematics (NSF grant DMS-1045536).

http://www.siam.org/journals/siap/73-4/89540.html

†Department of Mathematics, Harvey Mudd College, Claremont, CA 91711 (tum_chaturapruek@hmc.edu). This author's work was supported in part by Harvey Mudd College and by the Royal Thai Government through a Royal Thai Scholarship from the Development and Promotion of Science and Technology Talents Project (DPST).

‡Department of Mathematics, Pomona College, Claremont, CA 91711 (jonah.breslau@gmail.com). This author's work was funded by NSF grant DMS-1045536.

§Department of Mathematics, University of California, Los Angeles, Los Angeles, CA 90095 (danielyazdi@ucla.edu, sgmccalla@gmail.com). The third author's work was funded by NSF grant DMS-1045536. The fifth author's work was supported by ARO MURI grant W911NF-11-1-0332, ARO grant W911NF1010472, and NSF grant DMS-0968309.

¶Mathematics and Statistics, Dalhousie University, Halifax B3H 3J5, NS, Canada (tkolokol@gmail.com). This author's work was supported by a grant from AARMS CRG in Dynamical Systems and by NSERC grant 47050.

The UCLA model [33] incorporates the empirically observed phenomena of repeat/near-repeat events and the "broken windows" effect [39]. Repeat and near-repeat events refer to the self-exciting nature of burglary. For a short time after a home is burglarized, it becomes a more likely target for another burglary within the next few weeks; this is a repeat event. Additionally, the adjacent and nearby houses also become more likely targets for a future burglary; this is a near-repeat event. This effect is clearly seen in the burglary data, and even the temporal and spatial decay of the increased burglary likelihood can be observed [8, 17, 32, 18, 19]. Once a thief has successfully burgled a home, the thief knows how to break in, how to navigate the neighborhood, and what other valuables are available to steal [32, 40]. A great deal of research has been done to understand this phenomenon [9, 19, 2, 35, 28, 7, 18]. The "broken windows" effect accounts for the diffusive nature of crime. Neighborhoods with high crime exude a sense of lawlessness, and a notion of crime tolerance. As a result, such neighborhoods can become more desirable targets for burglars.

Another assumption of the UCLA model is that criminals travel through space according to a random walk biased toward attractive burglary sites. In a discrete setting, this amounts to criminals moving only to adjacent homes with each time step, or in a continuous setting, spreading according to a biased diffusion. Under this assumption, burglars only have access to a single mode of transportation and have knowledge that is restricted to the homes directly adjacent to them. This assumption is expected to be an oversimplification for human motion. It has been argued that animal movements, including those of humans, generate Lévy flights instead of random walks [11, 26, 15, 6]. A Lévy flight enables an animal to more efficiently explore its territory for resources than a random walk does. Instead of restricting movement only to neighboring sites, Lévy flights exhibit long range jumps. The probability of a long jump is dictated by a power-law distribution, and Brownian motion is equivalent to a Lévy flight with sufficiently strong decay in the distribution. These occasional long jumps interspersed with a local random walk can be seen in a typical daily commute in a big city. A commuter may first walk to a bus which takes a "flight" to a different part of the city; the commuter then resumes walking to work, perhaps detouring to grab a coffee. The nonlocal nature of this motion allows criminals to more efficiently examine the space for potential homes to rob, but it also assumes the criminals have knowledge extending far beyond their immediate surroundings.

While the criminal motion cannot be observed directly, the distance between criminals' homes and their targets is well known for solved crimes. This data indicates that burglars are willing to travel longer distances for more attractive targets and employ different means of transportation to make these long trips. In [22, 34, 38, 29, 12], it is seen that burglars are willing to travel longer distances for high-value targets. For example, Hesseling [12] found that in inner-city Utrecht most of the solved crimes were committed by outsiders who do not live in the inner-city. They travel to these central neighborhoods in Utrecht because they are more amenable, or attractive, for committing crimes. Once they make these long jumps, they then search locally for targets.

Different types of criminals exhibit significantly different mobility patterns. For example, as was shown in [34, 38], professionals and older burglars will travel farther than amateurs or younger burglars. One of the main reasons younger criminals do not travel as far is because they do not have access to cars and must commit their crimes on foot, bike, or public transportation. A drug addict committing crimes to feed his addiction will tend to target the first site he sees. Drug addicts might then follow a

Brownian motion when attempting a property crime. A group of professionals, however, will plan their crime and travel long distances to target a particularly appealing target, such as a bank. They then could reasonably be expected to follow a Lévy flight. The form of an offender's motion will also necessarily depend on the geography of their home territory, and the mobility patterns of criminals in Los Angeles will not match those in Halifax. For these reasons, it is important to understand how different mobility patterns will affect the dynamics in the UCLA model.

The goal of this paper is to extend the UCLA model to incorporate the "nonlocal" movement of criminals. We will specifically focus on motion by Lévy flights biased towards attractive burglary sites. As in the original UCLA model [33], we start with an agent-based cellular automata model; this is derived in section 2. By taking the continuum limit, we obtain a system of two PDEs for the criminal density and the attractiveness field. Unlike the original model, the resulting PDE for the criminal density is nonlocal, whereas the equation describing the attractiveness field remains local. Specifically, the new model contains the fractional Laplacian, a nonlocal extension of the normal Laplacian which allows for the superdiffusion of criminals. We perform a linear stability analysis (Turing analysis) around a homogeneous crime steady state and supplement this with numerical simulations that illustrate the effect of nonlocality on hotspot formation. We find that increasing the nonlocality can either increase or decrease the number of hotspots, depending on the parameter regime. Additionally, it can stabilize or destabilize the homogeneous steady state. We conclude our study with an asymptotic construction of the hotspot profile under criminal Lévy flights in a singular regime.

**2. Modeling biased Lévy flights.** In this section, we derive a modified version of the UCLA model to incorporate the criminal motion based on biased Lévy flights. We begin with a review of the original agent-based model from [33]. The agent-based model consists of stationary burglary sites, which exist on a one-dimensional grid with grid spacing $l$, and a collection of mobile burglars that travel from site to site. Accompanying each burglary site $k$ is a dynamic "attractiveness" $A_k(t)$; this, as the name implies, refers to the burglar's beliefs about the target site's value and ease of burglary and is proportional to the rate of burglary at the site. The agent-based game unfolds through discrete time steps $\delta t$ starting with some initial distribution of criminals at each burglary site. Each time step, every burglar in the system either chooses to move from his location to another location or to commit a crime. Burglaries are treated as random events that occur with probability

$$p_k(t) = 1 - e^{-A_k(t)\delta t}$$

at site $k$ in the time interval from $t$ to $t+\delta t$ for each burglar. The expected number of criminal events from a single burglar in the time interval $\delta t$ is then $A_k(t)\delta t$. If there are on average $N_k(t)$ burglars at site $k$ between $t$ and $t+\delta t$, then there should be $\delta t A_k N_k$ burglaries on average.

In the original UCLA model, the burglars could move only to neighboring sites. We allow the criminals to undergo a nonlocal flight to distant, but more attractive, burglary sites. These long jumps are biased by $A_k(t)$. If the criminal decides to commit a crime, he is then removed from the system as he returns home with his stolen goods. At each grid location and time step, burglars are added back with rate $\Gamma$ to account for their return to an active criminal state.

The attractiveness field can be decomposed into a static background term $A_0$ plus

a dynamic term $B_k(t)$:

$$A_k(t) \equiv A_0 + B_k(t). \tag{1}$$

The dynamic term accounts for the self-exciting nature of burglary: once a site has been burglarized, it and its neighbors are far more likely to undergo a repeat or near-repeat event. The dynamic term $B_k(t)$ depends on the previous burglaries at the site $k$ as well as the recent burglaries in the neighboring sites. These quantities depend on both the historical attractiveness at these sites and the number of crimes that occur at these sites. We thus let $E_k(t)$ denote the number of crimes at each location $k$ during the time interval $(t, t+\delta t)$, and define the expected number of criminals $N_k(t)$ to be the average number of criminals at site $k$ between $t$ and $t+\delta t$. If we neglect near-repeat victimization, then $B_k(t)$ should evolve according to

$$B_k(t+\delta t) = B_k(t)(1 - w\delta t) + \theta E_k(t),$$

where $\delta t$ is a characteristic time scale and the parameter $w$ represents the decay rate of the dynamic attractiveness field. $\theta$ is the proportionality constant that ties the number of crimes at a site to the rise in attractiveness at the site. The expected value of the attractiveness can be similarly expressed by replacing $E_k(t)$ with the expected number of crimes at the site $\delta t A_k N_k$. The evolution of the expected value for the dynamic attractiveness term with near-repeat events is then modeled following [33] as

$$B_k(t+\delta t) = \left[(1-\hat{\eta})\, B_k(t) + \frac{\hat{\eta}}{2}\left(B_{k-1} + B_{k+1}\right)\right](1 - w\delta t) + \delta t A_k N_k \theta. \tag{2}$$

Here, $\frac{\hat{\eta}}{2}\left(B_{k-1} + B_{k+1}\right)$ represents the "broken windows" effect whereby the attractiveness of a given area is affected by the attractiveness of its neighbors, and $0 < \hat{\eta} < 1$ is the strength of this effect. The term $\delta t A_k N_k$ is the mass-action law; it represents the total number of burglaries that took place in the time interval $[t, t+\delta t]$ at site $k$. Following [33], in (2) as well as in what follows, the densities $B_k$, $A_k$, and $N_k$ are understood to be expected values, i.e., averaged over all possible realizations.

Lévy flights represent a random motion whereby a particle takes steps whose distribution obeys a power law. For criminal motion, these steps should be biased toward areas with a high attractiveness $A$. Thus we define the relative weight of a criminal moving from point $i$ to point $k$, where $i \neq k$, as

$$w_{i\to k} = \frac{A_k}{l^{\mu}\,|i-k|^{\mu}}. \tag{3}$$

Here $\mu$ is the exponent of the underlying power law for the Lévy flight. The key feature is that the weight includes the attractiveness field $A$. The transition probability of a criminal moving from point $i$ to point $k$, where $i \neq k$, is then given by

$$q_{i\to k} = \frac{W_{i\to k}}{\sum_{j\in\mathbb{Z}, j\neq i} W_{i\to j}}. \tag{4}$$

As in [33], we assume that the burglars obey the following simple rules: during the time interval $\delta t$, the burglar either commits a crime with probability $A_i \delta t$ or else moves on according to a biased flight; new criminals appear with rate $\Gamma$. The equation that governs the expected number of criminals at each site from their densities at each

location in a previous time step can be derived by noting that criminals can only appear at site $k$ by moving there from some site $i$, as is governed by $q_{i\to k}$, or by birth with probability $\Gamma\delta t$. These rules for the criminal population are encoded as

$$N_k(t+\delta t) = \sum_{i\in\mathbb{Z}, i\neq k} N_i \cdot (1 - A_i\delta t) \cdot q_{i\to k} + \Gamma\delta t. \tag{5}$$

We now take the continuum limit for $\delta t, l \ll 1$. Let $N(x,t) = N_k(t)$, where $x = kl$. Similarly define $A(x,t)$ and $B(x,t)$ such that (2) becomes

$$\begin{aligned} A(x,t+\delta t) - A_0 \\ = \left[(1-\hat{\eta})\, A(x,t) + \frac{\hat{\eta}}{2}\left(A(x-l,t) + A(x+l,t)\right)\right](1 - w\delta t) + \delta t A N\theta. \end{aligned} \tag{6}$$

Using a Taylor expansion and keeping only the leading-order terms, we find the equation

$$A_t = \frac{l^2\hat{\eta}}{2\delta t} A_{xx} - w(A - A_0) + AN\theta. \tag{7}$$

Due to the nonlocal criminal movement, the derivation of the continuum limit for $N$ is more involved. We define

$$z := 2\sum_{k=1}^{\infty} \frac{1}{k^\mu} = 2\zeta(\mu) \tag{8}$$

and

$$\mathcal{L}f_i := \sum_{j\in\mathbb{Z}, j\neq i} \frac{f_j - f_i}{|j-i|^\mu\, l^\mu}. \tag{9}$$

Additionally, we write

$$\begin{aligned} \sum_{j\in\mathbb{Z}, j\neq i} w_{i\to j} &= \sum_{j\in\mathbb{Z}, j\neq i} \frac{A_j - A_i}{l^\mu\,|i-j|^\mu} + \sum_{j\in\mathbb{Z}, j\neq i} \frac{A_i}{l^\mu\,|i-j|^\mu} \\ &= A_i l^{-\mu} z + \mathcal{L}A_i \end{aligned}$$

so that

$$q_{i\to k} \sim \frac{A_k}{|i-k|^\mu}\left(\frac{1}{zA_i} - \frac{\mathcal{L}A_i l^\mu}{A_i^2 z^2}\right). \tag{10}$$

We then have

$$\frac{N_k(t+\delta t) - N_k(t)}{\delta t} = \frac{1}{\delta t}\left(\sum_{i\in\mathbb{Z}, i\neq k} N_i(1 - A_i\delta t) q_{i\to k} - N_k\right) + \Gamma \tag{11}$$

and expand to find

$$\sum_{i\in\mathbb{Z},i\neq k} N_i(1-A_i\delta t)q_{i\to k} - N_k \tag{12}$$

$$= \sum_i N_i\left(1-A_i\delta t\right)\frac{A_k}{|i-k|^\mu}\left(\frac{1}{zA_i}-\frac{\mathcal{L}A_i l^\mu}{A_i^2 z^2}\right) - N_k$$

$$= A_k\left(\left\{\sum_i \frac{N_i}{A_i}\left(1-A_i\delta t\right)\frac{1}{z\,|i-k|^\mu}\right\} - \frac{N_k}{A_k}\right) \tag{13}$$

$$- \sum_i N_i\left(1-A_i\delta t\right)\frac{A_k}{|i-k|^\mu}\frac{\mathcal{L}A_i l^\mu}{A_i^2 z^2}$$

$$\sim A_k\sum_i\left[\frac{\frac{N_i}{A_i}-\frac{N_k}{A_k}}{|i-k|^\mu\, z} - \frac{N_i}{|i-k|^\mu}\left(\frac{\mathcal{L}A_i l^\mu}{A_i^2 z^2}\right) - \delta t\frac{N_i}{|i-k|^\mu\, z}\right] \tag{14}$$

$$\sim A_k\left[\frac{l^\mu}{z}\mathcal{L}\left(N_k/A_k\right) - N_k\frac{\mathcal{L}A_k l^\mu}{A_k^2 z} - \delta t N_k\right]. \tag{15}$$

Note that we used $N_k = \sum_{i\neq k}\frac{N_k}{z|i-k|^\mu}$ in step (14); we only kept $O(l^\mu,\delta t)$ terms while ignoring any $O(l^\mu\delta t, l^{2\mu})$ terms.

The term $\mathcal{L}A_k$ is approximated using a Riemann sum as follows:

$$\mathcal{L}A_k = \sum_{j\in\mathbb{Z},j\neq k}\frac{A_j-A_k}{|j-k|^\mu\, l^\mu} = \frac{1}{l}\sum_{j\in\mathbb{Z},j\neq k}\frac{A(y_j)-A(x)}{y_j-x}l \sim \frac{1}{l}\int_{-\infty}^{\infty}\frac{A(y)-A(x)}{|y-x|^\mu}dy, \tag{16}$$

where we write $x = kl$, $y_j = jl$, $A_j = A(y_j)$, and $A_k = A(x)$. Next we write this operator in terms of the fractional Laplacian. We use the following definition of the fractional Laplacian in dimension $d$, from [21]:

$$-(-\Delta)^s f(x) := C_{d,2s}\int_{y\in\mathbb{R}^d}\frac{f(x)-f(y)}{|x-y|^{2s+d}}dy, \quad C_{d,2s} = 2^{2s}\frac{\Gamma\left(s+d/2\right)}{\pi^{d/2}|\Gamma(-s)|}, \quad 0<s\leq 1. \tag{17}$$

In order to simplify the notation for the remainder of this paper, we write

$$-(-\Delta)^s \text{ as } \Delta^s. \tag{18}$$

Normalizing the operator by $C_{d,2s}$ leads to a simple form for $\Delta^s$ in Fourier space [21, 41, 13]:

$$\mathcal{F}_{x\mapsto q}\left\{\Delta^s f(x)\right\} = -|q|^{2s}\mathcal{F}_{x\mapsto q}\{f(x)\}. \tag{19}$$

Note that the case $s = 1$ (i.e., $\mu = 3$ in one dimension) reduces to the usual Laplacian. We will use (19) both for the following numerical simulations and the stability analysis in section 3.

For convenience, we define the parameter

$$s := \frac{\mu-1}{2} \tag{20}$$

so that in one dimension

$$l\mathcal{L}A_k \sim C_{1,2s}^{-1}\Delta^s(A)$$

and

$$\sum_{i\in\mathbb{Z},i\neq k} N_i(1-A_i\delta t)q_{i\to k} - N_k \sim \frac{l^{\mu-1}}{z}C_{1,2s}^{-1}\left[A\Delta^s\left(\frac{N}{A}\right) - \frac{N}{A}\Delta^s(A)\right] - \delta t AN.$$

The continuum limit of (5) then becomes

$$\frac{\partial N}{\partial t} = \frac{l^{\mu-1}}{\delta t}\frac{\pi^{1/2}2^{1-\mu}|\Gamma\left(\frac{1-\mu}{2}\right)|}{z\Gamma(\mu)}\left[A\Delta^s\left(\frac{N}{A}\right) - \frac{N}{A}\Delta^s(A)\right] - AN + \Gamma. \tag{21}$$

Finally, we rescale variables to eliminate the parameters $w$ and $\theta$ from the equations as follows: $A = \bar{A}w,\ N = \rho w/\theta,\ t = \bar{t}/w$. Dropping the bars, we obtain

$$\frac{\partial A}{\partial t} = \eta A_{xx} - A + \alpha + A\rho, \tag{22}$$

$$\frac{\partial \rho}{\partial t} = D\left[A\Delta^s\left(\frac{\rho}{A}\right) - \frac{\rho}{A}\Delta^s(A)\right] - A\rho + \beta, \tag{23}$$

where

(24)

$$s = \frac{\mu-1}{2} \in (0,1],\ \eta = \frac{l^2\hat{\eta}}{2\delta t w},\ D = \frac{l^{2s}}{\delta t}\frac{\pi^{1/2}2^{-2s}|\Gamma(-s)|}{z\Gamma(2s+1)w},\ \alpha = \frac{A_0}{w},\ \text{and}\ \beta = \frac{\Gamma\theta}{w^2}.$$

To validate the continuum model, we perform direct numerical simulations of the agent-based model (1)–(5) and the continuum model (22), (23). Implementing the cellular automata model is straightforward: we consider a lattice of $n$ points and set $A_k, B_k, N_k = 0$ whenever $k \notin \{1,\dots,n\}$ in (1)–(5). Due to the nonlocal motion of criminals, each time step in the discrete model takes $O(n^2)$ time. For the continuum model, we employ a spectral method in space based on the fast Fourier transform (FFT) with the method of lines in time. We first discretize $A$ and $\rho$ in space using $K$ meshpoints; then we solve the $2K$ coupled ODEs in time. To approximate $\Delta^s u$, we make use of property (19) in Fourier space. On the interval $x \in [0, L]$, this is done through the FFT, as illustrated in the following MATLAB code:

```
K = numel(u); % u is a 1 by K array ;
q = 2*pi/L*[0:K/2-1, -K/2:-1];
laplaces_u = ifft(-abs(q).^(2*s).*fft(u));
```

The FFT enables us to calculate one time step in the continuum model in $O(K \log K)$ time, where $K$ is the number of gridpoints in the discretization. This computation assumes periodic boundary conditions for the solution.

Figure 1 shows a comparison between the numerical simulations for the discrete and continuous models. Excellent agreement is observed away from the boundaries. Near the boundaries, some disagreement is expected as the discrete case was not performed with periodic boundary conditions (incorporating more realistic boundary conditions for the continuum model is discussed in [41] but is outside the scope of this paper). Eventually, the pattern settles into a steady state consisting of two hotspots.

Figure 2 compares the eventual steady state of the discrete and continuum models for several different values of $\mu$. Good agreement is observed across the broad range of $\mu$.

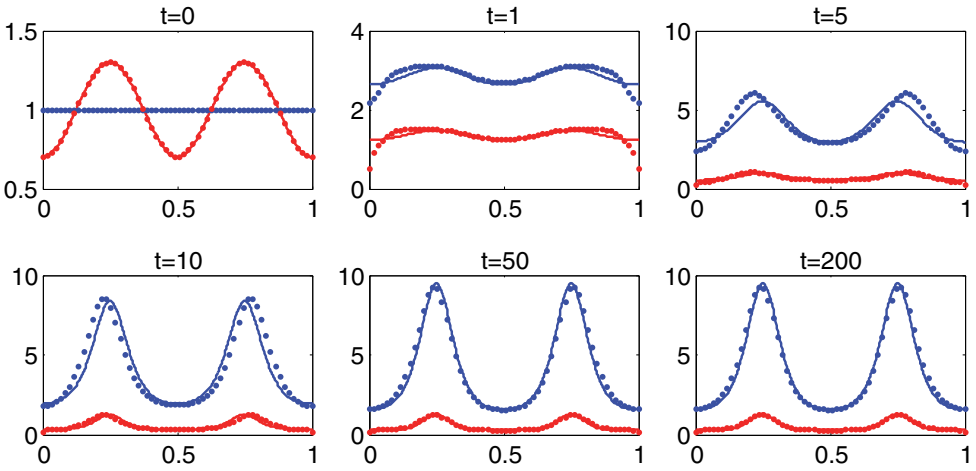


FIG. 1. *Simulations of a discrete model* (1)–(5) *and its continuum limit* (22), (23). *The discrete model is shown with dots, and the continuum model is shown with solid curves. For* $t \geq 1$, *the top curve is* $A$ *(blue online), and the bottom curve is* $N$ *(red online). The initial conditions (at* $t = 0$*) are taken to be* $A = 1$ *and* $N = 1 - 0.3\cos(4\pi x)$. *Parameters for the discrete model are* $\mu = 2.5$, $n = 60$, $l = 1/60$, $\hat{\eta} = 0.1$, $\delta t = 0.01$, $A_0 = 1$, $\Gamma = 3$. *The corresponding parameters for the continuum model are computed from* (24) *as* $s = 0.75$, $\eta = 0.001388$, $D = 0.1828$, $\alpha = 1$, $\beta = 3$.

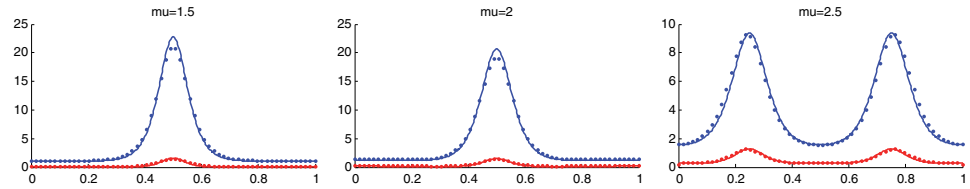


FIG. 2. *Comparison of the steady state obtained using the discrete model* (1)–(5) *and its continuum limit* (22), (23). *The parameters of the discrete model* (1)–(5) *are the same as in Figure* 1, *except for* $\mu$ *as indicated. The snapshots are taken at* $t = 200$, *by which time the solution has converged to the steady state.*

From (24), we find that $\eta^{-s}D = O((1-s)^{-1}(\delta t)^{s-1}) \gg 1$ for $0 < s \leq 1$ (the factor $(1-s)^{-1}$ comes from expanding $|\Gamma(-s)| \sim 1/(1-s)$ in the limit $s \to 1^-$). Thus, in the physically relevant regime $0 < s \leq 1$, the following condition holds:

$$\eta^{-s}D \gg 1, \quad 0 < s \leq 1. \tag{25}$$

In analogy with regular diffusion ($s = 1$), we refer to this condition as the "*separation of scales*"; it implies that the criminals $\rho$ diffuse much faster than the activation field $A$, and it plays a key role in the Turing analysis as well as the asymptotic construction of the hotspots below.

**3. Turing instability.** We now perform a linear Turing analysis around the homogeneous steady state of (22), (23) given by

$$\bar{A} = \alpha + \beta, \quad \bar{\rho} = \frac{\beta}{\alpha + \beta}. \tag{26}$$

Perturbing from the steady state (26), we write

$$A(x,t) = \overline{A} + \phi e^{\lambda t} e^{ikx}, \qquad \rho(x,t) = \overline{\rho} + \psi e^{\lambda t} e^{ikx}, \tag{27}$$

and look for a relationship between the different Fourier modes and the eigenvalues $\lambda$. Using (19), we have

$$\Delta^s e^{ikx} = -|k|^{2s} e^{ikx},$$

which yields the eigenvalue problem

$$\begin{bmatrix} -\eta|k|^2 - 1 + \bar{\rho} & \bar{A} \\ \frac{2\bar{\rho}}{\bar{A}} D|k|^{2s} - \bar{\rho} & -D|k|^{2s} - \bar{A} \end{bmatrix} \begin{bmatrix} \phi \\ \psi \end{bmatrix} = \lambda \begin{bmatrix} \phi \\ \psi \end{bmatrix}. \tag{28}$$

The dispersion relationship $\lambda = \lambda(k)$ is then given by

$$\lambda^2 - \tau\lambda + \delta = 0, \tag{29}$$

where

$$\tau = -D|k|^{2s} - \eta|k|^2 - \bar{A} - 1 + \bar{\rho} \quad \text{and} \quad \delta = D|k|^{2s}\left(\eta\,|k|^2 + 1 - 3\bar{\rho}\right) + \eta\,|k|^2\,\bar{A} + \bar{A}. \tag{30}$$

Figure 3 illustrates the effects of changing the strength of the Lévy walk decay exponent $s$ on the stability of the homogeneous steady state. There are five distinct possible regimes labelled (a) through (e) in the figure.

To determine the stability of the steady state (26), first note that $\tau < 0$. This implies that the steady state is stable if $\delta > 0$. In particular, we have stability if $\bar{\rho} < 1/3$ (i.e., $\alpha > 2\beta$). On the other hand, an instability occurs if $\delta < 0$ or

$$\bar{A} < D|k|^{2s}\left(-1 + \frac{3\bar{\rho}}{\eta\,|k|^2 + 1}\right) \text{ for some } k. \tag{31}$$

By computing the maximum of the right-hand side of this equation, we obtain the following characterization of the stability.

PROPOSITION 3.1. *Suppose that $\alpha > 2\beta$ (i.e., $\bar{\rho} < 1/3$). Then the homogeneous equilibrium* (26) *is stable. Suppose that $\bar{\rho} > 1/3$ and $\bar{A} < \bar{A}_*$, where*

$$\bar{A}_* := D\eta^s x^s \left(-1 + \frac{3\bar{\rho}}{x+1}\right) \tag{32}$$

*and where $x$ is the unique positive root of*

$$x^2 + x\,(2 + 3\bar{\rho}(1-s)/s) + 1 - 3\bar{\rho} = 0. \tag{33}$$

*Then the equilibrium* (26) *is unstable.*

Note that the boundary between the stable and the unstable steady state is given by $\bar{A} = \bar{A}_*$. Figure 4 illustrates the predictive value of Proposition 3.1. The dashed curve shows the boundary $\bar{A} = \bar{A}_*$ between instability and stability. The homogeneous steady state is stable above the curve and unstable below it. The numerical simulations for the full nonlocal equation agree very well with the linear

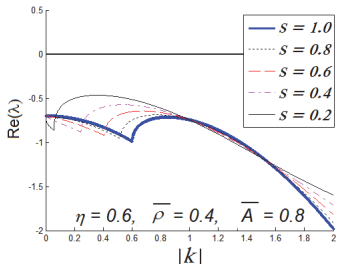


(a) A stable regime.

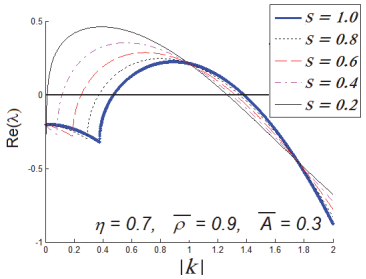


(b) An unstable regime.

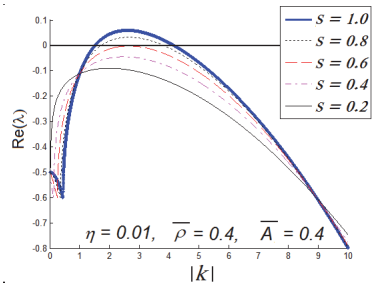


(c) Fractional diffusion leads to stability.

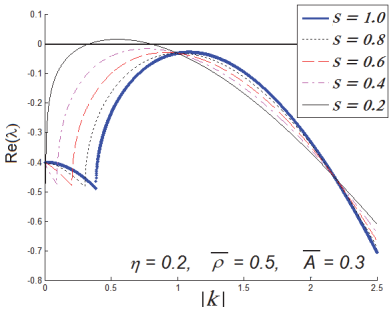


(d) Fractional diffusion leads to instability.

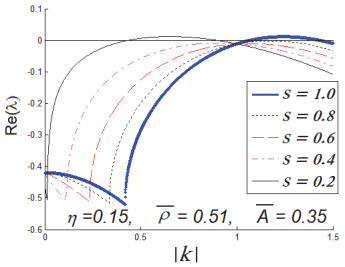


(e) Fractional diffusion leads to stability and then instability.

FIG. 3. *Different possible effects from fractional diffusion on the dispersion relation* (29). *A positive value for* $\mathrm{Re}(\lambda)$ *corresponds to an unstable homogeneous steady state.*

predictions; the exceptions, which are the crosses above the dashed line (red online), all lie very close to the bifurcation boundary.

Next we concentrate on the physically relevant parameter regime $\eta^{-s}D \gg 1$. Equation (31) implies that the equilibrium (26) is unstable for all modes of order $k = O(\eta^{-1/2})$, provided that $\bar{\rho} > 1/3$ and $\bar{A}, \bar{\rho} = O(1)$. To compute the dominant unstable mode, we change variables $k = x^{1/2}\eta^{-1/2}$ and let $M = D\eta^{-s} \gg 1$. We then obtain

$$\tau = -Mx^s - x + \bar{\rho} - 1 - \bar{A} \quad \text{and} \quad \delta = Mx^s(x + 1 - 3\bar{\rho}) + x\bar{A} + \bar{A}.$$

The fastest growing mode corresponds to the maximum of the dispersion curve, when $\lambda = (\partial\delta/\partial x) / (\partial\tau/\partial x)$. A posteriori analysis shows that in the limit $M \gg 1$, $x$ scales

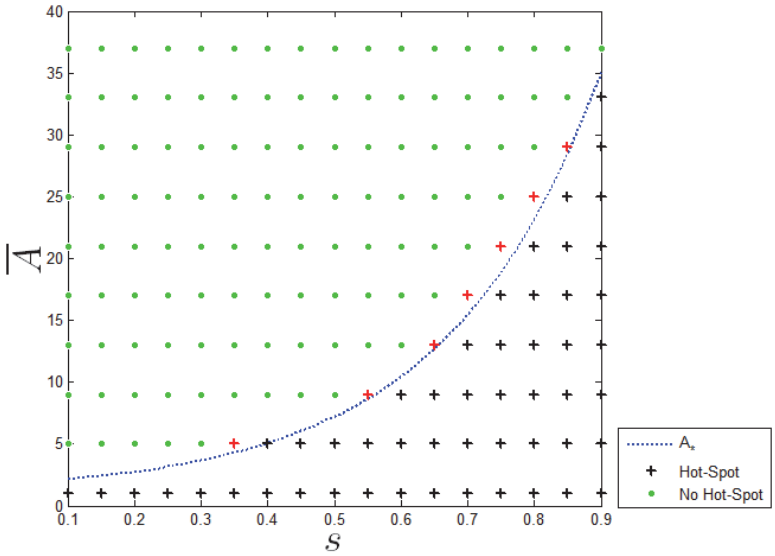


FIG. 4. *Comparison between the predicted instability threshold given by Proposition* 3.1 *and direct numerical simulations of the continuum model* (22), (23). *Parameter values are* $\eta = 0.001$, $\bar{\rho} = 1$, $D = 1$. *Crosses above the dashed line denote inconsistencies between the two approaches.*

like $x = O(M^{-1/(s+1)})$ so that $\lambda \sim -1 + 3\bar{\rho} - x\frac{s+1}{s}$ and the leading terms in (29) are

$$s^2\bar{\rho}(-2 + 3\bar{A} + 6\bar{\rho}) - Msx^{s+1} \sim 0. \tag{34}$$

This yields

$$x \sim \left[s\bar{\rho}(-2 + 3\bar{A} + 6\bar{\rho})M^{-1}\right]^{\frac{1}{s+1}}, \quad M \gg 1,$$

so that

$$k_{\text{fastest}}(s) \sim \left[\frac{s\bar{\rho}(-2 + 3\bar{A} + 6\bar{\rho})}{D\eta}\right]^{\frac{1}{2(s+1)}}, \quad D\eta^{-s} \gg 1. \tag{35}$$

We summarize as follows.

PROPOSITION 3.2. *Suppose that* $D\eta^{-s} \gg 1$, *with* $\alpha, \beta = O(1)$. *Then the homogeneous equilibrium* (26) *is stable if* $\alpha > 2\beta$ *and is unstable if* $\alpha < 2\beta$. *In the latter case, the most unstable mode is asymptotically given by* (35).

Formula (35) provides a way of obtaining a rough estimate of the total number of expected hotspots. Namely, on a domain of size $L$ with periodic boundary conditions, an instability of the form (27) has $kL/(2\pi)$ maxima. If each of these maxima eventually forms a fully developed hotspot, then the total number of maxima from the perturbation (27) can be approximated as

$$\text{expected number of maxima} \approx \text{floor}\left(\frac{L}{2\pi}k_{\text{fastest}}\right). \tag{36}$$

As illustrated in Figure 5, this typically overpredicts the final number of hotspots. Equation (36) relies on a linear analysis near the homogeneous equilibrium to predict the eventual number of hotspots. However, hotspots are localized patterns in the

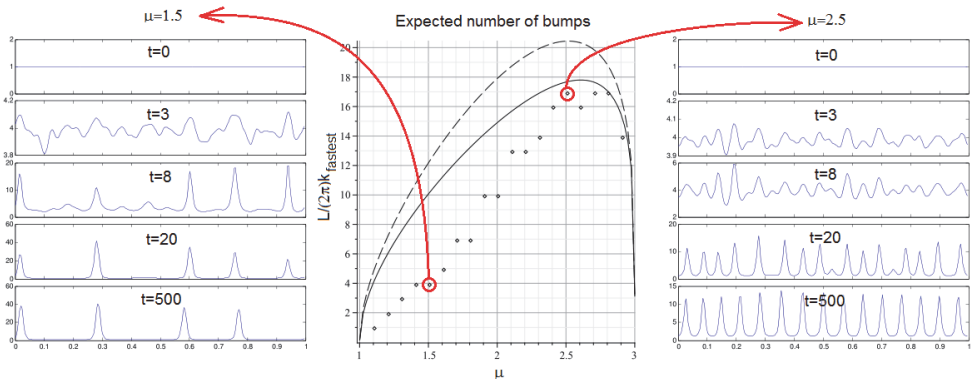


FIG. 5. *Center: Number of hotspots as a function of the Lévy walk decay exponent $\mu$. The dashed curve represents the asymptotics as given by* (35)*; the solid curve is the exact prediction from the dispersion relationship given by $k = x^{1/2}\eta^{-1/2}$, where $x$ satisfies* (34)*; the dots represent the observed number of hotspots from the full numerical simulation of the continuum model* (22), (23)*. Parameters of the continuum model are as given by* (24) *with $L = 1$ and with $l = 0.01$, $\delta t = 0.05$, $\hat{\eta} = 0.02$, $A_0 = 1$, $\Gamma = 3$, $w = \theta = 1$. Left: Snapshots of the simulation of the continuum model starting with small random fluctuations about the steady state. Initially, around 11 "bumps" form at $t = 3$. However, eventually only four hotspots are left at $t = 500$ due to a coarsening process. Right: Simulations with $\mu = 2.5$. Unlike in the figure on the left, the initial number of "bumps" is similar to the eventual number of hotspots.*

nonlinear regime far from the homogeneous equilibrium, and as such, there is no a priori reason to expect a Turing analysis to predict the eventual number of hotspots. Nonetheless, as Figure 5 illustrates, the Turing analysis appears to provide an upper bound for the number of stable hotspots in the nonlinear regime.

In terms of the model's original parameters, the dominant unstable mode (35) can be written as

$$k_{\text{fastest}}(\mu) \sim \frac{1}{l}\left[\frac{1}{|\Gamma\left(\frac{1-\mu}{2}\right)|}\left\{\frac{(\mu-1)\,\Gamma(\mu)\,\bar{\rho}(-2+3\bar{A}+6\bar{\rho})zw^2\,(\delta t)^2}{\hat{\eta}\pi^{1/2}2^{1-\mu}}\right\}\right]^{\frac{1}{\mu+1}}.$$

Note that the term in curly braces is $O((\delta t)^2) \ll 1$. Because of this, the maximum of this function is attained near $\mu \sim 3$. This is seen by expanding $|\Gamma\left(\frac{1-\mu}{2}\right)| \sim 2/(3-\mu)$ as $\mu \to 3^-$. We then obtain

$$k_{\text{fastest}}(\mu) \sim \frac{1}{l}\left[(3-\mu)\varepsilon\right]^{\frac{1}{\mu+1}}, \tag{37}$$

$$\text{where } \varepsilon := (\delta t)^2\,\frac{8\bar{\rho}(-2+3\bar{A}+6\bar{\rho})zw^2}{\hat{\eta}\pi^{1/2}}, \quad 0 < 3-\mu \ll 1.$$

The maximum of (37) is at $\mu_{\text{optimal}} \sim 3 - x$, where $x$ satisfies the transcendental equation

$$x = \frac{4}{1+\ln\frac{1}{\varepsilon x}}.$$

To leading order, we therefore obtain

$$\mu_{\text{optimal}} \sim 3 - \frac{2}{\ln(1/\delta t)}. \tag{38}$$

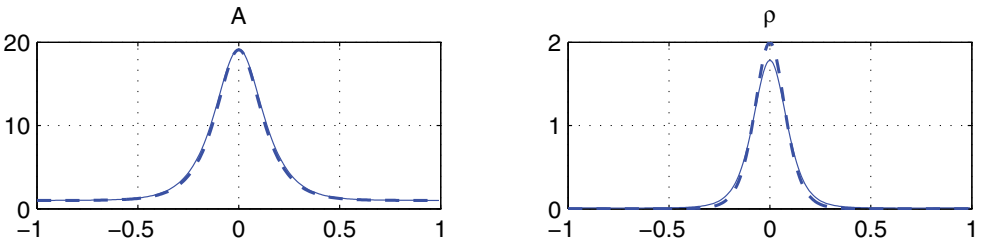


FIG. 6. *A single hotspot equilibrium solution to* (39) *for parameter values* $s = 0.5$, $\eta = 0.01$, $D = 1/\eta$, $\beta = 3$, $\alpha = 1$, $L = 1$. *The solid curve shows the full numerical simulations of the continuum model* (22), (23). *The dashed line shows the asymptotic approximation for* $A$ *and* $\rho$ *as derived in Proposition* 4.1.

**4. Asymptotic hotspot profile.** As Figure 5 illustrates, a Turing instability often leads to the formation of localized pulses, herein referred to as hotspots, rather than dispersion-type waves. In the singular limit where the diffusion of attractiveness is much less than the diffusion of criminals, the profile of the localized pulse can be understood. The profile and stability of these spots were studied in [20] for the standard diffusion case $s = 1$. Here, we generalize the basic construction of the hotspot performed in [20] to our Lévy flight model; the stability of these pulses is left for future work. We seek a symmetric steady state on the domain $[-L, L]$ in the form of a single spike centered at zero. The desired solution is illustrated in Figure 6. Such steady states on the domain $x \in [-L, L]$ satisfy

$$\begin{aligned} 0 &= \eta A_{xx} - A + \alpha + A\rho, \\ 0 &= D\left[A\Delta^s\left(\frac{\rho}{A}\right) - \frac{\rho}{A}\Delta^s(A)\right] - A\rho + \beta, \end{aligned} \tag{39}$$

with the additional conditions

$$A(x) = A(-x) \quad \text{and} \quad \rho(x) = \rho(-x).$$

First, we concentrate on the inner region, near $x = 0$, at the interior of the spike. Changing variables

$$x = \sqrt{\eta}y,$$

we find

$$0 = A_{yy} - A + \alpha + A\rho, \qquad 0 = D\eta^{-s}\left[A\Delta_y^s\left(\frac{\rho}{A}\right) - \frac{\rho}{A}\Delta_y^s(A)\right] - A\rho + \beta.$$

We recall that the assumption on the relative diffusion of attractiveness and criminals implies

$$D\eta^{-s} \gg 1.$$

Then the leading-order terms in (39) yield

$$A\Delta_y^s\left(\frac{\rho}{A}\right) - \frac{\rho}{A}\Delta_y^s(A) \sim 0.$$

This equation has solution

$$\rho = v_0 A^2,$$

where $v_0$ is still to be determined. The inner problem becomes

$$0 \sim A_{yy} - A + \alpha + A^3 v_0.$$

The self-consistent ansatz

$$v_0 = O(\eta) \ll 1$$

follows from the following computations. Assuming that $\alpha = O(1)$, we then have

$$A(y) \sim v_0^{-1/2} w(y),$$

where $w$ satisfies the ground state equation

$$w_{yy} - w + w^3 = 0, \quad w \to 0 \text{ as } |y| \to \infty, \quad w'(0) = 0.$$

This ground state has a well-known homoclinic orbit which can be computed explicitly as

$$w(y) = \sqrt{2}\,\mathrm{sech}(y).$$

It remains to determine $v_0$. To do so, we integrate the second equation in (39). For any two functions $u, v$, note that

$$\int \left[u\Delta^s(v) - v\Delta^s(u)\right] dx = C \int\int \frac{u(x)\left(v(y)-v(x)\right) - v(x)\left(u(y)-u(x)\right)}{|x-y|^{2s+1}} dxdy = 0;$$

thus we obtain

$$\int_0^L A\rho dx = \int_0^L \beta dx = \beta L. \tag{40}$$

To estimate the left-hand side, we make the assumption that $A\rho \ll 1$ in the outer region away from the spike. This leads to

$$\begin{aligned}\int_0^L A\rho dx &\sim \int_0^\infty A^3(y) v_0 \eta^{1/2} dy \sim \eta^{1/2} v_0^{-1/2} \int_0^\infty w^3 dy \\ &\sim \eta^{1/2} v_0^{-1/2} \pi/\sqrt{2},\end{aligned}$$

which yields

$$v_0^{-1/2} \sim 2^{1/2} \beta L \eta^{-1/2}/\pi. \tag{41}$$

To verify the assumption that $A\rho \ll 1$, we again change variables

$$\rho = vA^2$$

with $v(0) = v_0$. Then (39) becomes

$$D\left[A\Delta^s(Av) - Av\Delta^s(A)\right] - A^3 v + \beta = 0 = \eta A_{xx} - A + \alpha + A^3 v. \tag{42}$$

To be self-consistent, we need $A^3 v \ll O(1)$ in the outer region. Then $A \sim \alpha = O(1)$ such that in the outer region we obtain

$$D\Delta^s v - \alpha v + \beta/\alpha^2 \sim 0.$$

From (41), note that $v_0 = O(\eta)$; this suggests a rescaling $v = \hat{v}\eta$ in the outer region giving $D\eta\Delta^s\hat{v} + \beta/\alpha^2 \sim 0$ with $\hat{v}(0) = 2^{1/2}\beta L/\pi = O(1)$. It follows that if $D\eta \geq O(1)$, then $\hat{v} = 0(1)$ and we find $A^3 v = O(\eta) \ll O(1)$ as desired. In conclusion, the self-consistency condition is precisely $D\eta \geq O(1)$. We summarize as follows.

PROPOSITION 4.1. *Consider a single hotspot on the interval $[-L, L]$. Suppose that $D\eta^{-s} \gg 1$ and $D\eta \geq O(1)$, with $\alpha, \beta = O(1)$. Then the spike profile in the inner region satisfies*

$$A \sim \frac{2}{\pi}\beta L\eta^{-1/2}\operatorname{sech}(x\eta^{-1/2}), \qquad |x| \leq O(\eta^{1/2}), \tag{43}$$

$$\rho \sim 2\operatorname{sech}^2(x\eta^{-1/2}). \tag{44}$$

*In the outer region $|x| \gg O(\eta^{1/2})$, we have $A \sim \alpha$.*

Note that a solution for $A$ that is uniformly valid in both the inner and outer regions is

$$A \sim \left(\frac{2}{\pi}\beta L\eta^{-1/2} - \alpha\right)\operatorname{sech}(x\eta^{-1/2}) + \alpha. \tag{45}$$

A sample verification of Proposition 4.1 is displayed in Figure 6: the asymptotic expression (45, 44) is compared to the numerically computed steady state with good agreement.

**5. Discussion.** As seen in Figure 5, there is an optimal value of the Lévy flight exponent $\mu_{\text{optimal}} \in (1, 3]$ which leads to the largest number of hotspots. Note that this is not the same as maximizing the amount of crime: at the equilibrium state, the total amount of crime is given by $\int A\rho$ and is independent of $\mu$, as was shown in (40). On the other hand, the total number of criminals $\int \rho$ *is* proportional to the number of hotspots, as is evident from Proposition 4.1; see formula (44), which is independent of the spot radius $L$. Thus $\mu_{\text{optimal}}$ is the exponent which maximizes the total number of criminals. Intuitively, if the criminals move too fast or too sporadically (smaller $\mu$), they will miss some opportunities for looting. On the other hand, they will also miss opportunities if they move very little ($\mu$ close to 3). The best strategy should therefore be a compromise between widely exploring the state space and exploring localized niches. Besides "maximizing" the number of criminals, having many hotspots potentially makes life more difficult for the police: as noted in [30], patrolling strategies typically take crime locations into account, as opposed to simply randomly patrolling the streets. Having more hotspots to patrol can thus put more strain on limited police resources, even if the total amount of crime is the same. Note that the optimal value of $\mu_{\text{optimal}} \sim 3 - \frac{2}{\ln(1/\delta t)}$ as computed in (38) is relatively close to a random walk and Brownian motion $\mu = 3$.

The physical constraints of the model naturally lead to the *separation of scales* $\eta^{-s}D \gg 1$ in the continuum model (see (25)). This same condition naturally arises in the asymptotic construction of the hotspot (Proposition 4.1). Additionally, this condition is necessary in Proposition 3.2 which provides a sharp threshold boundary $\alpha \sim 2\beta$ for the Turing instability. Under the natural assumption $\eta^{-s}D \gg 1$, it is expected that the hotspot solutions will coexist with dispersion-type waves when $\alpha < 2\beta$. In particular, we expect a subcritical bifurcation of the homogeneous steady state at the bifurcation point as $\alpha \to 2\beta$ from below. This observation is consistent with the analysis in [20] (see Figure 7 therein), as well as the weakly nonlinear analysis in [30] for the standard diffusion case $s = 1$.

While this paper concentrates on one-dimensional hotspots, we have also performed numerical simulations in two dimensions for the cellular automata model to see the effect of a biased Lévy flight. These simulations indicate that, similarly to the one-dimensional case, the amplitude and number of hotspots vary with the exponent $\mu$.

Lévy flights crucially produce fractional Laplacians in the continuous limit. Fractional Laplacians have a particularly simple Fourier transform (19) which makes it possible to efficiently solve the corresponding nonlocal PDEs numerically through the FFT. This property also enables an analytical computation of the Turing instability. It would be interesting to generalize the computations of this paper to more realistic models of human locomotion [11, 26, 6]. In [11, 26], it is suggested that the spatial step sizes are distributed according to a truncated Lévy flight with an inner cutoff radius near the origin where the steps are uniformly distributed, and an outer cutoff radius where the step sizes are exponentially distributed; the power law distribution is observed in between the two radial cutoffs. Such a model is easy to implement in the cellular automata model: the weights (3) are replaced with $W_{i\to k} = A_k f(l|i-k|)$, where

$$f(r) = \begin{cases} 1, & r < r_1, \\ (r/r_1)^{-\mu}, & r_1 < r < r_2, \\ (r_2/r_1)^{-\mu} \exp(-(r-r_2)\,\nu), & r > r_2, \end{cases}$$

and $r_1, r_2$, $\mu, \nu > 0$ are appropriately chosen parameters. Unfortunately, such a choice of $f(r)$ does not have a simple expression for its Fourier transform, which makes it harder to analyze. Nonetheless, our formulation of the biased walk can be extended to more general models and more realistic spatial networks. Moreover, we expect that the leading-order asymptotic construction of the hotspot profile will not depend on the precise form of $f(r)$.

As shown in Figure 5, the Turing instability does not predict the eventual number of hotspots. These structures are in the fully nonlinear regime and are typically far from the Turing instability threshold. Instead, the stability theory for spike-type solutions as developed in [14] needs to be extended to the nonlocal case. For the original model with a biased Brownian motion of criminals, this has been done in [20]. Extending the theory to biased Lévy flights remains an open question.

**Acknowledgments.** We thank Andrea Bertozzi for fruitful discussions and suggestions. We also thank the anonymous referees for useful remarks that helped to improve the paper.

REFERENCES

[1] D. Beavon, P. L. Brantingham, and P. J. Brantingham, *Crime Prevention Studies*, Vol. 2, Willow Tree Press, Monsey, NY, 1994.
[2] W. Bernasco and P. Nieuwbeerta, *How do residential burglars select target areas? A new approach to the analysis of criminal location choice*, Br. J. Criminol., 45 (2005), pp. 296–315.
[3] A. E. Bottoms and P. Wiles, *Explanations of time and place*, in Crime, Policing and Place: Essays in Environmental Criminology, Routledge, New York, 1992, pp. 11–35.
[4] P. Brantingham and P. Brantingham, *Criminality of place*, Eur. J. Crim. Policy Res., 3 (1995), pp. 5–26.
[5] P. J. Brantingham and P. L. Brantingham, *Patterns in Crime*, Macmillan, New York, 1984.
[6] D. Brockmann, L. Hufnagel, and T. Geisel, *The scaling laws of human travel*, Nature, 439 (2006), pp. 462–465.

[7] J. E. Eck, S. Chainey, J. G. Cameron, M. Leitner, and R. E. Wilson, *Mapping Crime: Understanding Hot Spots*, National Institute of Justice, Washington, DC, 2005.
[8] G. Farrell and K. Pease, *Repeat Victimization*, Criminal Justice Press, Monsey, New York, 2001.
[9] G. Farrell, C. Phillips, and K. Pease, *Like taking candy: Why does repeat victimization occur?*, Br. J. Criminol., 35 (1995), pp. 384–399.
[10] M. K. Felson, *Crime and Nature*, Sage Publications, Thousand Oaks, CA, 2006.
[11] M. C. Gonzalez, C. A. Hidalgo, and A. L. Barabasi, *Understanding individual human mobility patterns*, Nature, 453 (2008), pp. 779–782.
[12] R. B. P. Hesseling, *Using data on offender mobility in ecological research*, J. Quant. Criminol., 8 (1992), pp. 95–112.
[13] B. D. Hughes, M. F. Shlesinger, and E. W. Montroll, *Random walks with self-similar clusters*, Proc. Natl. Acad. Sci. USA, 78 (1981), pp. 3287–3291.
[14] D. Iron, M. J. Ward, and J. Wei, *The stability of spike solutions to the one-dimensional Gierer–Meinhardt model*, Phys. D, 150 (2001), pp. 25–62.
[15] A. James, M. J. Plank, and A. M. Edwards, *Assessing Lévy walks as models of animal foraging*, J. R. Soc. Interface, 8 (2011), pp. 1233–1247.
[16] S. D. Johnson, *Repeat burglary victimisation: A tale of two theories*, J. Exp. Criminol., 4 (2008), pp. 215–240.
[17] S. D. Johnson, W. Bernasco, K. J. Bowers, H. Elffers, J. Ratcliffe, G. Rengert, and M. Townsley, *Space-time patterns of risk: A cross national assessment of residential burglary victimization*, J. Quant. Criminol., 23 (2007), pp. 201–219.
[18] S. D. Johnson and K. J. Bowers, *The stability of space-time clusters of burglary*, Br. J. Criminol., 44 (2004), pp. 55–65.
[19] S. D. Johnson, K. Bowers, and A. Hirschfield, *New insights into the spatial and temporal distribution of repeat victimization*, Br. J. Criminol., 37 (1997), pp. 224–241.
[20] T. Kolokolnikov, M. Ward, and J. Wei, *The Stability of Steady-State Hot-Spot Patterns for a Reaction-Diffusion Model of Urban Crime*, preprint, arXiv:1201.3090v1 [nlin.PS], 2012.
[21] Y. Nec, *Spike-type solutions to one dimensional Gierer–Meinhardt model with Lévy flights*, Stud. Appl. Math., 129 (2012), pp. 272–299.
[22] M. O'Leary, *Modeling criminal distance decay*, Cityscape, 13 (2011), pp. 161–198.
[23] J. H. Ratcliffe and M. J. McCullagh, *Hotbeds of crime and the search for spatial accuracy*, Geogr. Syst., 1 (1999), pp. 385–398.
[24] J. H. Ratcliffe and G. F. Rengert, *Near-repeat patterns in Philadelphia shootings*, Security J., 21 (2008), pp. 58–76.
[25] G. F. Rengert, *The journey to crime*, in Crime, Policing and Place: Essays in Environmental Criminology, Routledge, New York, 1992, pp. 109–117.
[26] I. Rhee, M. Shin, S. Hong, K. Lee, S. J. Kim, and S. Chong, *On the Lévy-walk nature of human mobility*, IEEE/ACM Trans. Netw., 19 (2011), pp. 630–643.
[27] D. W. Roncek and R. Bell, *Bars, blocks, and crimes*, J. Environ. Syst., 11 (1981), pp. 35–47.
[28] A. Sagovsky and S. D. Johnson, *When does repeat burglary victimisation occur?*, Aust. N. Z. J. Criminol., 40 (2007), pp. 1–26.
[29] P. Santtila, M. Laukkanen, A. Zappal, and D. Bosco, *Distance travelled and offence characteristics in homicide, rape, and robbery against business*, Legal Criminol. Psych., 13 (2008), pp. 345–356.
[30] M. B. Short, A. L. Bertozzi, and P. J. Brantingham, *Nonlinear patterns in urban crime: Hotspots, bifurcations, and suppression*, SIAM J. Appl. Dyn. Syst., 9 (2010), pp. 462–483.
[31] M. B. Short, P. J. Brantingham, A. L. Bertozzi, and G. E. Tita, *Dissipation and displacement of hotspots in reaction-diffusion models of crime*, Proc. Natl. Acad. Sci. USA, 107 (2010), pp. 3961–3965.
[32] M. B. Short, M. D'Orsogna, P. J. Brantingham, and G. E. Tita, *Measuring and modeling repeat and near-repeat burglary effects*, J. Quant. Criminol., 25 (2009), pp. 325–339.
[33] M. B. Short, M. R. D'Orsogna, V. B. Pasour, G. E. Tita, P. J. Brantingham, A. L. Bertozzi, and L. B. Chayes, *A statistical model of criminal behavior*, Math. Models Methods Appl. Sci., 18 (2008), pp. 1249–1267.
[34] B. Snook, *Individual differences in distance travelled by serial burglars*, J. Investig. Psych. Offender Profil., 1 (2004), pp. 53–66.
[35] M. Townsley, R. Homel, and J. Chaseling, *Infectious burglaries. A test of the near repeat hypothesis*, Br. J. Criminol., 43 (2003), pp. 615–633.
[36] A. Tseloni and K. Pease, *Repeat personal victimization. 'Boosts' or 'flags'?*, Br. J. Criminol., 43 (2003), pp. 196–212.
[37] A. Tseloni and K. Pease, *Repeat personal victimization: Random effects, event dependence and unexplained heterogeneity*, Br. J. Criminol., 44 (2004), pp. 931–945.

[38] P. J. Van Koppen and R. W. J. Jansen, *The road to the robbery: Travel patterns in commercial robberies*, Br. J. Criminol., 38 (1998), pp. 230–246.
[39] J. Q. Wilson and G. L. Kelling, *Broken windows and police and neighborhood safety*, Atlantic Mon., 249 (1982), pp. 29–38.
[40] R. Wright and S. Decker, *Burglars on the Job*, Northeastern University Press, Boston, 1994.
[41] A. Zoia, A. Rosso, and M. Kardar, *Fractional Laplacian in bounded domains*, Phys. Rev. E, 76 (2007), 021116.